

Title	Efficient searching for grain storage container by combine robot
Author(s)	Kurita, Hiroki; Iida, Michihisa; Suguri, Masahiko; Masuda, Ryohei; Cho, Wonjae
Citation	Engineering in Agriculture, Environment and Food (2014), 7(3): 109-114
Issue Date	2014-07
URL	http://hdl.handle.net/2433/189412
Right	© 2014 Asian Agricultural and Biological Engineering Association. Published by Elsevier B.V.
Type	Journal Article
Textversion	author

Efficient Searching for Grain Storage Container by Combine Robot*

Hiroki KURITA*¹, Michihisa IIDA*², Masahiko SUGURI*³, Ryohei MASUDA*³, Wonjae CHO*¹

Abstract

In this study, a combine robot was equipped with an autonomous grain container searching function. In order to realize automated grain unloading, the combine robot has to search and identify the grain storage container in an outdoor environment. A planar board was attached to the container. The marker was searched for using a camera mounted on the unloading auger of the combine. An efficient marker searching procedure was proposed on the basis of a numerical analysis of the camera's field of view and was verified experimentally. The results showed that the combine robot efficiently searched for and detected the marker and positioned its spout at the target point over the container to unload the grain.

[Keywords] head-feeding combine robot, grain unloading operation, grain container searching operation, spout positioning, field of view

I Introduction

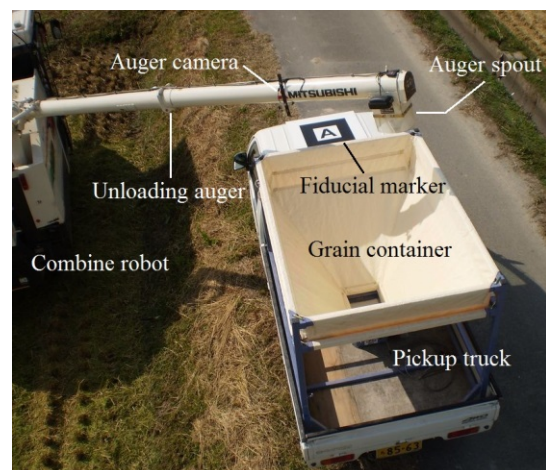
1 In Japan, the number of workers engaged in
2 agriculture is decreasing, and the average age of
3 agricultural workers is rapidly increasing. Food
4 self-sufficiency in Japan remains low compared to other
5 developed countries. Japan must improve its agricultural
6 productivity in order to maintain its sustainability. Field
7 robots are expected to play an important role in
8 improving the efficiency of agricultural operations and
9 meeting workforce shortages. Attempts to develop
10 automated agricultural machinery have previously been
11 reported (Noguchi and Terao, 1997; Ishida *et al.*, 1998;
12 Nagasaka *et al.*, 2004; Takai *et al.*, 2010). In a previous
13 study (Iida *et al.*, 2012), we robotized a head-feeding
14 combine harvester (hereafter referred to as a combine)
15 and used it to harvest rice and wheat in fields. The
16 combine robot successfully traveled along a target path
17 and harvested rice crops autonomously.

19 However, a human operator is needed to manually
20 control the combine and unload grain from its grain tank
21 into a separate grain storage container. We aimed to
22 automate the unloading operation as well. A pickup truck
23 is driven and parked by a human driver on a farm road.
24 The parking position of the truck is determined in
25 advance. As the combine robot can obtain this parking
26 position as Global Positioning Satellite (GPS) data, it

27 autonomously travels to a position near the truck when
28 the grain tank is full. However, the position of the
29 combine relative to the pickup truck is not strictly fixed,
30 because the human driver cannot perfectly park the
31 pickup truck without positional errors. Thus, the
32 combine robot has to find the pickup truck by an image
33 processing technique and then correct its relative
34 position to unload grain into the truck without any loss.

35 Kurita *et al.* (2012) utilized an image processing
36 technique to appropriately position the unloading auger
37 to unload grain. Figure 1 shows the assumed situation
38 for their concept.

39



40

41

Fig. 1. Setup of autonomous unloading operation.

* Partly presented at the 6th International Symposium on Machinery and Mechatronics for Agricultural and Biosystems Engineering ISMAB 2012

*1 JSAM Student Member, Graduate School of Agriculture, Kyoto University, Kitashirakawa Oiwake-cho, Sakyo-ku, Kyoto, 606-8502, Japan

*2 JSAM Member, Corresponding author, Graduate School of Agriculture, Kyoto University, Kitashirakawa Oiwake-cho, Sakyo-ku, Kyoto, 606-8502, Japan ; iida@elam.kais.kyoto-u.ac.jp

*3 JSAM Member, Graduate School of Agriculture, Kyoto University, Kitashirakawa Oiwake-cho, Sakyo-ku, Kyoto, 606-8502, Japan

1 A planar fiducial marker (aluminum board, 400 mm ×
 2 400 mm) is placed on the roof of the pickup truck to
 3 detect the position of the grain container. The position is
 4 extracted from images captured by the camera attached
 5 to the unloading auger. On the basis of the extracted
 6 image features, the positional relation between the
 7 combine and container is determined using image
 8 processing techniques. The experimental results showed
 9 that the auger spout can be visually positioned at the
 10 target point with sufficient accuracy. In addition to this
 11 basic concept, the combine robot is required to search
 12 for and detect the fiducial marker autonomously and
 13 accurately.

14 Another issue with searching for the marker is work
 15 efficiency. Because work efficiency is one of the most
 16 important concerns for the automation of agricultural
 17 machinery (Buckmaster and Hilton, 2005), agricultural
 18 operations using an autonomous machine should not
 19 take much longer than the time required to perform the
 20 same operation manually. Thus, the autonomous
 21 unloading system should be designed in such a manner
 22 that the fiducial marker can be located smoothly and
 23 integrated into the autonomous unloading operation as
 24 quickly as possible.

25 For efficiently locating a grain container, a camera is
 26 required to smoothly capture the fiducial marker. A
 27 combine robot should search for the marker so that the
 28 camera can sweep over as wide an area as possible
 29 without overlapping. Thus, the strategy for efficient
 30 marker searching is closely linked to the camera's field
 31 of view (FOV) and its coverage. In visual servoing, the
 32 coverage of the camera's FOV is quite important for
 33 optimal control of a robot vehicle or manipulator;
 34 therefore, it has been widely studied by researchers
 35 concerned with mobile robots (Zhang and Ostrowski,
 36 2002; Salaris *et al.*, 2011), especially those who have
 37 developed a robot that searches for a particular object
 38 (Tsotsos and Shubina, 2007). It is difficult to actually
 39 measure the FOV of the auger camera for any set of
 40 decisive parameters, while a numerical simulation can
 41 give the FOV for any parameter with ease. Thus, the
 42 objectives of this study were as follows: to compute the
 43 FOV of the auger camera against FOV parameters based
 44 on the pinhole camera model, propose a marker
 45 searching algorithm in order to efficiently search for and
 46 accurately detect the marker and examine the actual
 47 performance of the proposed method with a combine
 48 robot.

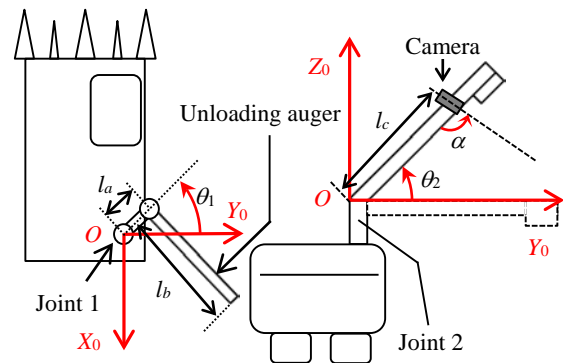
49

50 II Materials and Methods

51 1. Kinematic Modeling and Mechanics of 52 Unloading Auger

53 The test vehicle was a head-feeding combine harvester,
 54 VY50 CLAM (Mitsubishi Agricultural Machinery Co.,
 55 Ltd, Shimane, Japan). The unloading auger of the
 56 combine was modeled with a two-degrees-of-freedom
 57 manipulator consisting of two joints (joints 1 and 2). As
 58 illustrated in Fig. 2, a right-handed coordinate system
 59 was assigned to the combine; the x axis of the coordinate
 60 system was along the body of the combine in the
 61 direction opposite to the direction of its motion, and the z
 62 axis pointed vertically upward. The state of the
 63 unloading auger was determined by the two joint angles
 64 (hereafter θ_1 and θ_2). Joint 1 rotated at an angle of -110°
 65 $< \theta_1 < 200^\circ$. The grain could be discharged when -110°
 66 $< \theta_1 < 90^\circ$. However, unloading was expected to be
 67 performed when $20^\circ < \theta_1 < 90^\circ$. Joint 2 rotated at an
 68 angle of $0^\circ < \theta_2 < 45^\circ$.

69



70 Fig. 2. Kinematic model of unloading auger.

71

72

73 Joints 1 and 2 were actuated by a DC motor and
 74 hydraulic cylinder, respectively. Each joint rotated at a
 75 constant rate: 38.3 °/s for joint 1 and 20.7 °/s (upward)
 76 and 10.7 °/s (downward) for joint 2 with on-off control.
 77 Link lengths l_a , l_b , and l_c were defined as shown in Fig. 2.
 78 The camera's elevation angle α was set to 71° . Table 1
 79 lists the specifications of the camera.

80

81

Table 1. Camera specifications.

Model	UCAM-DLA200H (ELECOM)
Image sensor	1/4 in CMOS
Focal length	4.3 mm
F-number	1.8
Angle of view (diagonal)	60 °

82

2. FOV of Auger Camera

A rice paddy is usually enclosed by embankments and at least one farm road (see Fig. 3).

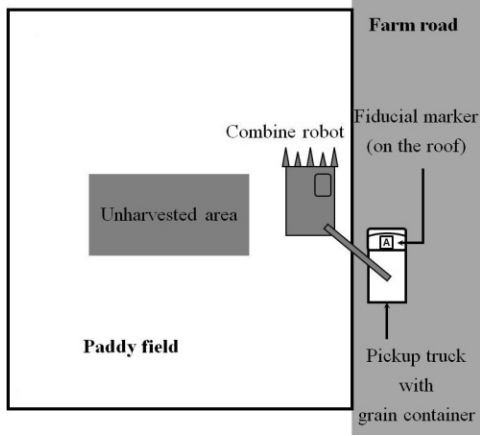


Fig. 3. Positional relation between the combine and the truck.

A commercialized head-feeding combine harvester is equipped with its unloading auger on the right side of the vehicle (see Fig. 3). As is the case for manned harvesting, the combine robot harvests rice crops in an anticlockwise fashion (Iida *et al.*, 2012). Thus, in this study, the truck was always located on the right side of the combine. Let h_{fr} be the height of the adjacent farm road from a paddy field, h_c be the height of joint 1 of the combine harvester, and h_{kt} be the height of the pickup truck.

In general, the FOV can be represented by its angle of view (AOV) and depth of field (DOF). The AOV comprises the vertical and horizontal AOV. The DOF represents the area of the visual scene that is acceptably sharp. Outside of this range, images are blurred. The DOF depends on the focal length of the camera. In this study, the focal length of the camera was kept constant so that the DOF would fall within an acceptable range of sharpness. The DOF was empirically determined; at the same time, the target plane (i.e., the roof of the truck) was experimentally confirmed to form an image with sufficient sharpness for the expected range of the height from the paddy field to the farm road h_{fr} . In this study, the range was assumed to be $0 \text{ m} < h_{fr} < 1.5 \text{ m}$.

A pinhole camera model (Gonzalez and Wintz, 1987; Xu and Zhang, 1996) was adopted for the following simulation. Further approximations were applied to the system model. In the following analysis, the unloading auger was dealt with as a line, not a solid object, and the camera's dimensions were neglected. Hence, l_a was assumed to be 0.0 m. The values l_b and l_c were 4.280 and 3.195 m, respectively. It may be considered that l_c is also

a decisive variable for the FOV. Obviously, the camera needs to be attached at the top of the unloading auger to obtain as large an FOV as possible. When attached to the spout, however, the camera cannot obtain a clear image because of the dust that flows out of the spout during the unloading operation. Thus, the camera was attached as close to the auger spout as possible without being obstructed by dust from the unloading operation. This position was empirically determined and regarded as constant throughout the study.

When h_c was longer than $h_{kt} + h_{fr}$, the associated parameters were as depicted in Fig. 4, which represents the cross-sectional view at the Y_0 - Z_0 plane when $\theta_1 = 90^\circ$.

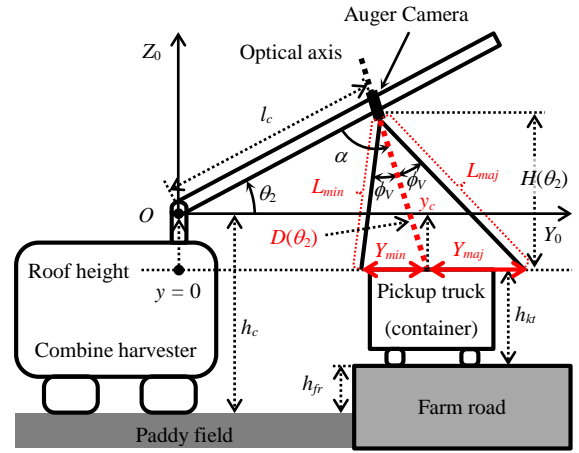


Fig. 4. Cross-sectional view at the Y_0 - Z_0 plane.

The value of ϕ_v is half that of the vertical AOV. The FOV at the height of the fiducial marker on the roof is divided by the optical axis (the point y_c in Fig. 4) into two parts; the lengths of these parts along the Y_0 axis are Y_{min} , which is closer to the combine, and Y_{maj} , which is farther. L_{min} and L_{maj} are the distances between the upper or lower edges of the FOV at the roof height and optical center, respectively. The depth of field at the marker plane $D(\theta_2)$ is represented as

$$D(\theta_2) = \frac{H(\theta_2)}{\sin(\theta_2 + \alpha)} \quad (1),$$

where $H(\theta_2)$ is $l_c \sin \theta_2 + (h_c - h_{fr} - h_{kt})$. Similarly, L_{min} and L_{maj} are obtained as follows:

$$L_{min} = \frac{H(\theta_2)}{\sin(\theta_2 + \alpha - \phi_v)} \quad (2).$$

$$L_{maj} = \frac{H(\theta_2)}{\sin(\theta_2 + \alpha + \phi_v)} \quad (3).$$

Then, Y_{min} and Y_{maj} are written as follows:

$$Y_{min} = \sqrt{\{D(\theta_2)\}^2 + L_{min}^2 - 2D(\theta_2)L_{min} \cos \phi_V} \quad (4).$$

$$Y_{maj} = \sqrt{\{D(\theta_2)\}^2 + L_{maj}^2 - 2D(\theta_2)L_{maj} \cos \phi_V} \quad (5).$$

2 The value of y_c is obtained geometrically using Eq. (6):

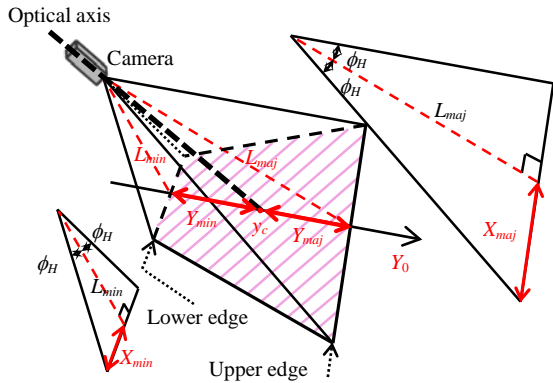
$$y_c = \sqrt{\{D(\theta_2)\}^2 + l_c^2 - 2D(\theta_2)l_c \cos \alpha} + \frac{h_c - h_{fr} - h_{kt}}{\tan(\theta_2 + \alpha)} \quad (6).$$

3 Figure 5 shows the FOV and parameters that are also
4 illustrated in Fig. 4. To make the figure clearer, the plane
5 including the line of L_{min} and the lower edge is clipped
6 and shown separately on the left side. Here, ϕ_H is half of
7 the horizontal AOV. X_{min} is half of the bottom length of
8 the rectangular triangle consisting of the angle ϕ_H and the
9 line segment with the length L_{min} . Hence,

$$X_{min} = L_{min} \tan \phi_H \quad (7).$$

10 Similarly, the plane that includes the line of L_{maj} and
11 the upper edge is depicted separately in the right side,
12 and X_{maj} is defined along with X_{min} .

$$X_{maj} = L_{maj} \tan \phi_H \quad (8).$$



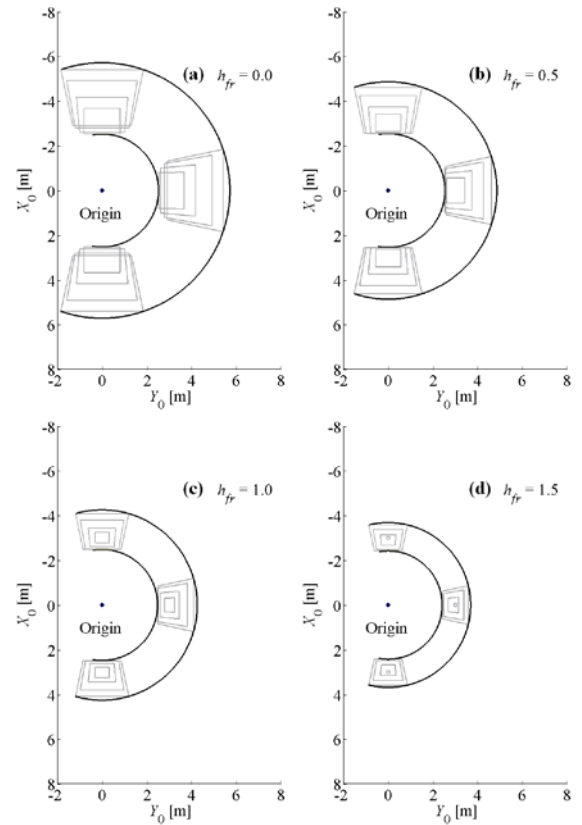
14 Fig. 5. Conceptual image of FOV.

15 Finally, the FOV can be simulated using the parameters
16 y_c , X_{min} , X_{maj} , Y_{min} , and Y_{maj} . When h_c is shorter than h_{kt} +
17 h_{fr} , the FOV can be simulated in a manner similar to the
18 case of $h_c > h_{kt} + h_{fr}$.
19
20
21

22 III Auger Control for Searching Operation

23 Figure 6 shows the maximal FOV for the
24 representative h_{fr} values of 0.0, 0.5, 1.0, and 1.5 m on the
25 combine-based coordinate system (i.e., $O-X_0Y_0Z_0$ in Fig.
26 2) when θ_1 of the unloading auger rotates from 180° to

27 0° . Note that the point $(X_0, Y_0) = (0, 0)$ in Fig. 6, which is
28 marked as *Origin*, indicates the origin of the
29 combine-based coordinate system. Especially for $\theta_1 = 0^\circ$,
30 90° , and 180° , the FOVs at $\theta_2 = 20^\circ, 30^\circ, 40^\circ$, and 45°
31 have a trapezoidal shape; among them, the FOV at 20° is
32 the narrowest and that at 45° is the widest. In short, each
33 maximal FOV shows the total area captured by the
34 camera when θ_2 varies from 20° to 45° . In Figs. 6(a) and
35 (b), the maximal FOV consists of the smallest FOV at θ_2
36 $= 20^\circ$ and largest FOV at $\theta_2 = 45^\circ$. As shown in Figs.
37 6(c) and (d), the maximal FOV is only generated by the
38 FOV at $\theta_2 = 45^\circ$ because it includes all of the FOVs at
39 the other θ_2 values. If searching is performed at $\theta_2 = 20^\circ$
40 and $\theta_2 = 45^\circ$, the camera searches the total area that it
41 can physically capture.
42



43 Fig. 6. Maximal FOV.

44 (a). $h_{fr} = 0.0$ m; (b). $h_{fr} = 0.5$ m;
45 (c). $h_{fr} = 1.0$ m; (d). $h_{fr} = 1.5$ m.
46
47

48 However, if the unloading auger rotates with $\theta_2 = 20^\circ$,
49 physical interference may arise between the auger and
50 grain storage container, especially when $h_{fr} = 1.5$ m.
51 Thus, the searching procedure should be performed at θ_2
52 $= 30^\circ$ and $\theta_2 = 45^\circ$. Because the maximal FOV can be
53 almost entirely covered using only the FOV at $\theta_2 = 45^\circ$,
54 the searching procedure should be performed primarily

1 at $\theta_2 = 45^\circ$ and then at $\theta_2 = 30^\circ$. Hereinafter, the former
 2 is *the primary searching step*, and the latter is *the*
 3 *secondary searching step*.

4 The entire searching procedure is as follows. First, the
 5 two joints of the unloading auger are kept at $\theta_1 = 192.0^\circ$
 6 and $\theta_2 = 2.6^\circ$, which is the state that the combine usually
 7 travels and harvests in (let this state be *the default*
 8 *position*). The auger moves upward to $\theta_2 = 45^\circ$ and
 9 rotates clockwise to $\theta_1 = 0^\circ$ (the primary step). The
 10 combine inevitably needs to keep $\theta_2 = 45^\circ$ for the
 11 rotation from the default position to prevent the
 12 unloading auger from crashing into the cab. Then, the
 13 auger drops down to $\theta_2 = 30^\circ$ and rotates anticlockwise
 14 to $\theta_1 = 90^\circ$ (the secondary step). If the marker is not
 15 detected, the auger returns to the default position. During
 16 the search, only the marker detection is performed with
 17 the image processing. When the fiducial marker is
 18 detected, the auger stops immediately and rests for 2 s to
 19 obtain clearer images, which are used to calculate the
 20 precise target joint angles. After that, positioning is
 21 performed.

22 More than 92% of the maximal FOV can be covered
 23 by the primary step; with the additional searching by the
 24 secondary step, a coverage of more than 98% is achieved.
 25 Since the unloading auger rotates at a regular rate, the
 26 maximum times required for the primary and secondary
 27 steps are 7.9 and 4.9 s, respectively. The auger stops for
 28 1 s to switch the searching mode from the primary step
 29 to the secondary step.

30

31 IV Field Experiment

32 We conducted an experiment to confirm the viability
 33 of the proposed searching-positioning method and to
 34 evaluate its efficiency. A combine robot was parked
 35 alongside a pickup truck, and a fiducial marker was
 36 placed on its roof (c.f. Fig. 1). We then ran the combine
 37 control program. The combine robot searched for the
 38 fiducial marker as described in Section III. After the
 39 marker was detected, the spout was positioned according
 40 to the basic concept. A series of searching-positioning
 41 operations was autonomously performed by the
 42 developed software program.

43 Two types of positional relations between the combine
 44 robot and fiducial marker were tested. In case 1, the
 45 marker was located in an area where it could be captured
 46 by the primary searching step. In case 2, the marker was
 47 located in an area where it could not be captured by the
 48 primary searching step but could be captured by the
 49 secondary searching step. We conducted the test three

50 times for each case and recorded the angular
 51 displacement and required time for spout positioning.

52 For test 1 of case 1 and test 3 of case 2, the heights of
 53 the farm road h_{fr} were 2.12 and 1.06 m, respectively,
 54 whereas h_{fr} was 0.00 m in the other tests. In addition, the
 55 position and orientation of the truck relative to the
 56 combine were the same for tests 2 and 3 of case 1 and
 57 tests 1 and 2 of case 2.

58

59

V Results and Discussion

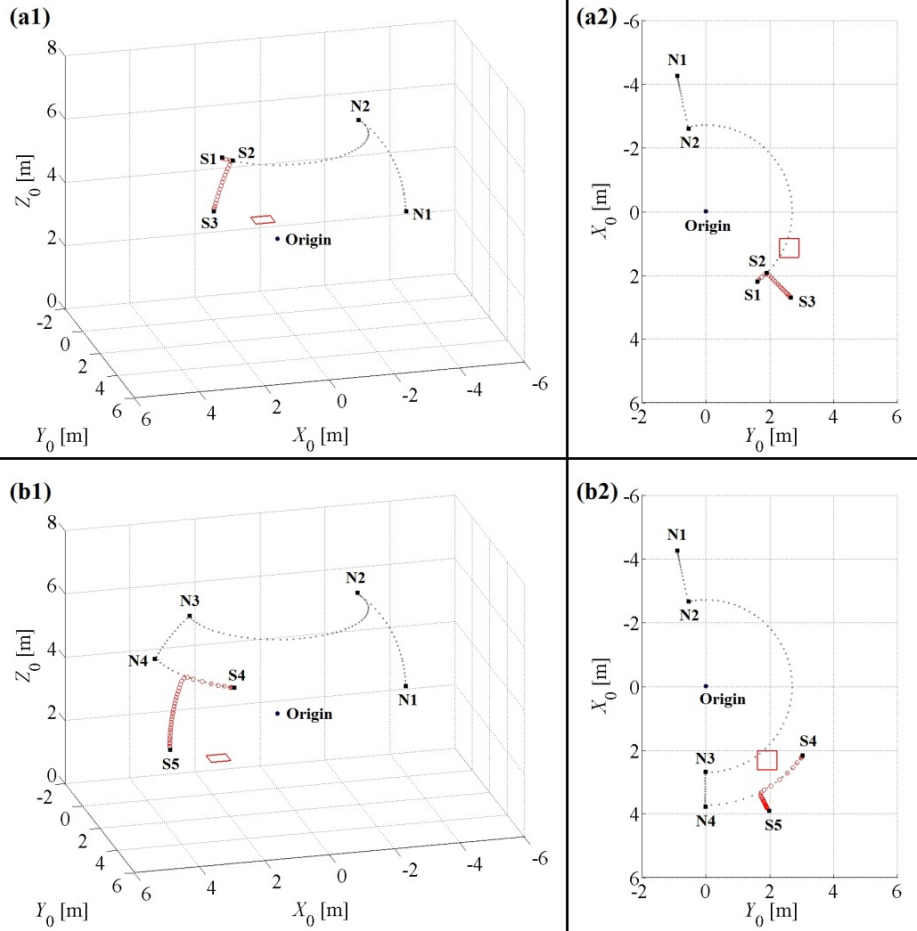
60 Figure 7 shows the experimental results for (a1, a2)
 61 case 1 and (b1, b2) case 2. The grey dotted line shows
 62 the locus of the auger spout during the searching process,
 63 while the red circle indicates the positioning process. The
 64 red rectangle represents the estimated position of the
 65 fiducial marker. As illustrated in Figs. 7(a1) and (b1), the
 66 primary step started its path from the default position
 67 (i.e., $\theta_1 = 192.0^\circ$ and $\theta_2 = 2.6^\circ$; marked as N1 in the
 68 figure). The unloading auger raised its joint angle θ_2 up
 69 to 45° (marked as N2) and then rotated clockwise until it
 70 reached the next node N3. During this rotation, the
 71 fiducial marker was successfully detected at the spout
 72 position S1 ($\theta_1 = 37.5^\circ$ and $\theta_2 = 45^\circ$). During the
 73 positioning, the auger rotated anticlockwise from S1 via
 74 S2 ($\theta_1 = 44.6^\circ$ and $\theta_2 = 45^\circ$) to S3 ($\theta_1 = 44.6^\circ$ and $\theta_2 =$
 75 29.8°). In this instance, it took 7.6 s for the fiducial
 76 marker to be detected. After 2.2 s of rest to obtain clearer
 77 images, the robot started the spout positioning, which
 78 took 2.0 s.

79 Figs. 7(b1) and (b2) show the results when the camera
 80 found the fiducial marker in the second searching step.
 81 After the end of the primary searching step (N3: $\theta_1 = 0^\circ$
 82 and $\theta_2 = 45^\circ$), the unloading auger lowered its joint angle
 83 θ_2 down to 30° (marked as N4) and then rotated
 84 anticlockwise to $\theta_1 = 90^\circ$. The fiducial marker was
 85 detected at the spout position S4 ($\theta_1 = 54^\circ$ and $\theta_2 = 30^\circ$).
 86 After a few seconds, the auger was positioned to $\theta_1 = 27^\circ$
 87 and $\theta_2 = 0^\circ$ (marked as S5). The primary searching step
 88 took 9.6 s, and it took 4.6 s from the end of the primary
 89 step for the fiducial marker to be detected. The
 90 positioning step took 3.6 s in this case. Overall,
 91 positioning took 23 s.

92 Table 2 summarizes the time required for the
 93 searching-positioning operation; three tests were
 94 performed for each case. The table also contains h_{fr} and
 95 the required angular displacement from the default
 96 position to the target position. Overall, θ_2 (up) was
 97 constant because the unloading auger was only raised at
 98 the beginning of the searching procedure.

1

2



3
4 Fig. 7. Trajectory of auger spout: (a1) overhead view and (a2) top view of case 1 trajectory; (b1) overhead view
5 and (b2) top view of case 2 trajectory.
6

7 Table 2. Required time for searching-positioning task.

Case	Test	Required time [s]	Angular displacement [°]			h_{fr} [m]
			θ_1	$\theta_2(\text{up})$	$\theta_2(\text{down})$	
1	1	12	147.4	42.4	15.2	2.12
	2	18	133.5	42.4	45.0	0.00
	3	17	133.9	42.4	45.0	0.00
2	1	23	218.6	42.4	45.0	0.00
	2	22	216.8	42.4	45.0	0.00
	3	16	205.9	42.4	30.6	1.06
Manual operation			37 s (on average)			

8

9 For case 1, test 1 clearly required less time. h_{fr} was
10 higher than for the other two tests with this case, and the
11 target point was also higher. Thus, the angular
12 displacement of θ_2 (down) was small. Compared to case
13 1, case 2 took longer as a whole. This is because case 2
14 required a larger angular displacement of θ_1 . However,

15 test 2 took 16 s, which was shorter than tests 2 and 3 of
16 case 1. It took longer for the auger to lower its angle than
17 in the other cases, as described in Section II-1. The
18 difference in the required displacement of θ_2 (down)
19 (30.6° in test 3 of case 2 while 45.0° in tests 2 and 3 of
20 case 1) was why this test provided better results.

21 A combine operator took about 37 s on average to
22 manually position the unloading auger to an appropriate
23 point above the grain container. This is the time needed
24 for actual unloading operation performed by not only
25 skilled but also unskilled operators. In comparison, our
26 proposed searching-positioning method is clearly more
27 efficient (18 s on average). As noted in Section III, the
28 primary searching step covers most of the maximal FOV.
29 In other tests we conducted, the marker was usually
30 detected in this step. Thus, the secondary step serves as
31 an auxiliary searching procedure. However, the addition
32 of the second step allows the auger camera to cover 98%
33 of the maximal FOV.

34

VI Summary

In order to realize efficient marker searching operation, the FOV of an auger camera was computed on the basis of decision variables associated with the FOV. Under the assumption that the marker is searched for by the auger camera, we proposed an efficient marker searching procedure on the basis of the simulation results.

The maximal FOVs at representative θ_2 values were computed. The simulation results indicated that 92% of the maximal FOV can be covered by searching at $\theta_2 = 45^\circ$ (the primary searching step), and 98% of the maximal FOV is covered by also searching at $\theta_2 = 30^\circ$ (the secondary searching step). The experimental results showed that the fiducial marker was mainly detected in the primary searching step. The secondary searching step was still useful for achieving the maximal FOV. The fiducial marker was detected when located inside the maximal FOV either during the primary or secondary searching step; additional searching steps were not needed. The combine robot accurately recognized the marker with the auger camera while rotating its unloading auger and then positioned its spout at the target point on the basis of the detected marker.

When the fiducial marker was detected in the primary searching step, the robot took 16 s on average for searching and positioning. It took 20 s on average when the fiducial marker was acquired in the secondary step. With the proposed method, the combine robot performed the searching-positioning task within 18 s on average, which is less than the time required for manual operation.

Therefore, the combine robot can use the proposed method to search, detect, and position with high efficiency and sufficient reliability.

References

Buckmaster, D. R. and Hilton, J. W. 2005. Computerized cycle analysis of harvest, transport, and unload systems. *Computer and Electronics in Agriculture* 47: 137-147.

Gonzalez, R. C. and Wintz, P. 1987. *Digital Image Processing* 2nd Edition. Addison-Wesley Publishing Company, MA, USA.

Iida, M., Uchida, R., Zhu, H., Suguri, M., Kurita, H. and Masuda, R. 2013. Path-following control for a head-feeding combine robot. *Engineering in Agriculture, Environment and Food* 6(2): 61-67.

Ishida, M., Imou, K., Okado, A., Takenaga, H., Honda, Y., Itokawa, N. and Shibuya, Y. 1998. Autonomous tractor for forage production. *Journal of the Japanese Society of*

Agricultural Machinery 60(2): 59-66.

Kurita, H., Iida, M., Suguri, M. and Masuda, R. 2012. Application of Image Processing Technology for Unloading Automation of Robotic Head-Feeding Combine Harvester. *Engineering in Agriculture, Environment and Food* 5(4): 146-151.

Nagasaka, Y., Umeda, N., Kanetani, Y., Taniwaki, K. and Sasaki, Y. 2004. Automated rice transplanter using global positioning and gyroscopes. *Computer and Electronics in Agriculture* 43: 223-234.

Noguchi, N. and Terao, H. 1997. Path planning of an agricultural mobile robot by neural network and genetic algorithm. *Computer and Electronics in Agriculture* 18: 187-204.

Salaris, P., Pallottino, L., Hutchinson, S. and Bicchi, A. 2011. From Optimal Planning to Visual Servoing with Limited FOV. In Proc. 2011 IEEE/RSJ International Conference on Intelligent Robots and Systems, 2817-2824. San Francisco, CA., 25-30 September.

Takai, R., Barawid, O. Jr., Ishii, K. and Noguchi, N. 2010. Development of Crawler-Type Robot Tractor based on GPS and IMU. Preprint of the IFAC International Conference on AGRICONTROL 2010, A3-5. Kyoto, Japan, 6-8 December.

Tsotsos, J. K. and Shubina, K. 2007. Attention and Visual Search: Active Robotic Vision Systems that Search. Keynote Lecture of the 5th International Conference on Computer Vision Systems, Bielefeld, Germany, 21-24 May.

Xu, G. and Zhang, Z. 1996. *Epipolar Geometry in Stereo, Motion and Object Recognition: A Unified Approach*. Norwell: Kluwer Academic Publishers.

Zhang, H. and Ostrowski, J. P. 2002. Visual Motion Planning for Mobile Robots. *IEEE Transactions on Robotics and Automation* 18(2), 199-208.